Journal of Materials Processing Tech. 307 (2022) 117681

Contents lists available at ScienceDirect

Journal of Materials Processing Tech.

journal homepage: www.elsevier.com/locate/jmatprotec

Internal crack formation in cross wedge rolling: Fundamentals and rolling methods

Tomasz Bulzak [a,*], Zbigniew Pater [a], Janusz Tomczak [a], Łukasz Wójcik [a], Alberto Murillo-Marrodán [b]

[a] Lublin University of Technology, Nadbystrzycka 36, Lublin 20-618, Poland
[b] Department of Mechanics, Design and Industrial Management, University of Deusto, Avda Universidades 24, Bilbao 48007, Spain

ARTICLE INFO

Associate Editor: Zhenshan Cui

Keywords:
Cross wedge rolling
Damage
Fracture
FEM
Experiment

ABSTRACT

Material fracture is a serious problem in cross wedge rolling (CWR). Finding new solutions for material fracture prevention in CWR processes presents a technological challenge for researchers these days. This paper presents a new approach to the problem of material fracture, which investigates a not previously undertaken aspect concerning the influence of the cross wedge rolling method on the development of internal cracks. CWR rolling methods in which two tools are used (two flat wedges, two roll wedges, roll wedge-concave segment, two concave wedges) were analysed. In addition, the effect of the number of moving tools on material fracture in CWR is investigated. Material fracture is predicted by a novel hybrid fracture criterion. In this paper, FE simulations were used to determine the value of the hybrid fracture criterion. Experimental studies were used to validate the built numerical model. The conducted research has shown that with the increase in the ovalization of the cross-section of the rolled forging, which depends on the rolling method and the number of moving tools, the degree of damage to the forging increases. The highest degree of damage occurs during the flat wedge rolling method, in which only one wedge is moving. The lowest degree of damage occurs when rolling with two moving concave wedges. The most important conclusion of the study is that changing the rolling scheme from the least favourable to the most favourable one allows to reduce the degree of forgings damage twice.

1. Introduction

Cross wedge rolling (CWR) is used to produce axisymmetric forgings and preforms. This manufacturing technique has many advantages such as high productivity, high accuracy, and reduced material consumption. Nevertheless, it also entails some disadvantages, the most serious being axial fracture. Numerous studies on material fracture prediction in CWR have been conducted recently. The development of a correct mathematical model for predicting material fracture in CWR would significantly improve the design of CWR technology and tools. Zhou et al. (2020a) proposed a fracture criterion based on the state of stress, specifically the maximum shear stress and maximum principal stress. According to this criterion, material fracture will occur in CWR when these stresses reach certain limit values. The share of individual stress components in the fracture criterion value depends on material constants, the sum of which is equal to 1.

Preliminary results obtained by Zhou et al. (2020a) showed that the maximum shear stress had a greater impact on the final value of the fracture criterion. Zhou et al. (2020b) verified their criterion using a material model composed of plasticine and flour. It was found that the criterion could be used to predict the initiation of material fracture in CWR. Pater et al. (2020a) proposed a hybrid fracture criterion in which the damage function also depended on the maximum shear stress and maximum principal stress. The share of individual stress components in the total value of the damage function was determined based on a stress triaxiality-dependent parameter. Unlike Zhou's stress-based fracture criterion, Pater's criterion was an energy criterion and thus depended on strain. Results obtained by Pater et al. (2020b) showed that the hybrid criterion could also be used for predicting material facture in CWR. Both fracture criteria were verified using the flat tool rolling method.

Material cracking in the cross-wedge rolling process has been the subject of many studies. The amount of research carried out in this area indicates that this is a very important issue. Elimination of the negative phenomenon of cracking will increase the technological capabilities of

* Corresponding author.
E-mail address: t.bulzak@pollub.pl (T. Bulzak).

https://doi.org/10.1016/j.jmatprotec.2022.117681
Received 19 March 2022; Received in revised form 7 June 2022; Accepted 15 June 2022
Available online 18 June 2022

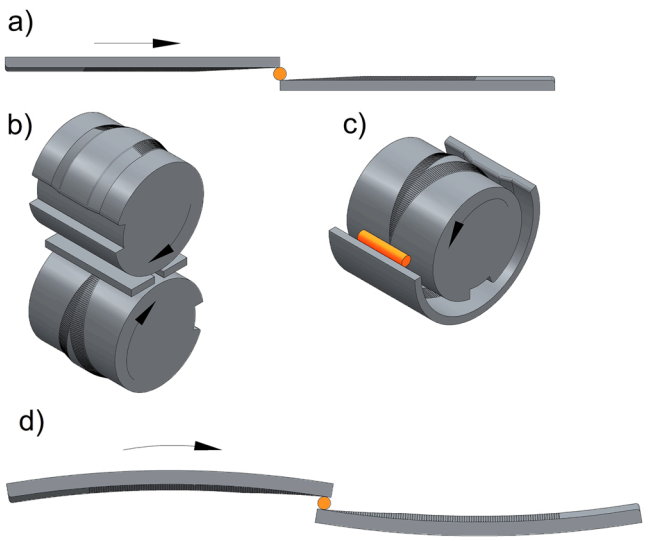

Fig. 1. Cross wedge rolling (CWR) methods: a) flat wedges – Method A, b) roll wedge – Method B, c) roll wedge-concave segment – Method C, d) two concave wedges – Method D.

the CWR process. Liu et al. (2014) and Yang et al. (2012) analysed the effect of the ratio of cross-section reduction in the CWR process on the formation of internal cracks. The results indicate that the best conditions for the CWR process occur for a cross-section reduction of around 50%. A great deal of attention has been focused on the influence of basic wedge tool parameters (α - forming angle, β - spreading angle) on crack formation. Zhou et al. (2012) conducted an evaluation of the effect of tool angle parameters on crack formation. The analysis shows that the forming angle should be as large as possible, while the spreading angle should be as small as possible. Huang et al. (2017) conducted a study on the warm and hot cross-wedge rolling process. The results obtained show that the formation of internal voids is less during warm rolling. Novella et al. (2014) obtained similar results during hot rolling of aluminium alloy AA6082, which cracked during rolling at higher temperatures.

Previous studies on material fracture in cross wedge rolling focused on two CWR methods. Novella et al. (2015) investigated the problem of ductile fracture in aluminium alloy in CWR conducted with two rolls. Huo et al. (2017) investigated material fracture in 2-roll CWR of railway axles. The mechanism of crack formation in the 2-roll CWR process conducted with the use of two rolls was also studied by Yang et al. (2018). Jia et al. (2012) examined the effect of tool parameters on internal void formation. Komischke et al. (2018) analysed the problem of material fracture in a cross rolling process conducted with specially designed roller segments. Jia et al. (2020) investigated the problem of material fracture in multi-wedge cross wedge rolling using cylindrical tools. Lee et al. (2008) assessed various ductile fracture criteria in terms of their application in modelling a cold CWR processes conducted with rotating tools. Carkicrcali et al. (2013) analysed the fracture of Ti6Al4V titanium alloy parts in cross wedge rolling performed on a rolling mill equipped with flat tools. Dong et al. (2000) analysed the stress state in terms of crack formation in cross wedge rolling with flat tools. Li et al. (2002) investigated the formation of internal defects in aluminium specimens in cross wedge rolling with flat tools. Silva et al. (2011) used Forge 2008 to model crack propagation in CWR with flat tools. Li and Lovell (2008) studied failure mechanisms in CWR using two rolling methods. In numerical modelling they used flat tools, while experiments were conducted with the use of cylindrical tools. However, they did not undertake to compare those two rolling methods.

The literature review shows that in research works and industrial processes, cross wedge rolling is conducted with the use of two flat wedges or two rolls. As far as flat wedges are concerned, rolling mills have one or two moving tools. This is due to the fact that only these two types of mills are available on the market. They are used in both industry and research centres for conducting research.

The literature review shows that material fracture in CWR is a serious problem. Findings from the studies conducted independently by the research teams led by Zhou et al. (2020a), (2020b) and Pater et al. (2020a), (2020b) make it possible to predict material fracture in CWR with great accuracy. Previous studies have investigated material fracture in rolling processes conducted with two flat tools or with two rolls, as described in Introduction. According to Fu and Dean (1993) and Li and Lovell (2004), five CWR methods can be distinguished. Four of them involve the use of two tools, while one method involves the use of three tools. There are no studies investigating the effect of CWR method on the material's susceptibility to cracking. This paper presents results of a study assessing the probability of crack formation depending on the applied rolling method. This study investigates only rolling methods based on the use of two tools. The three-tool rolling method is omitted in the analysis due to the fact that it has a different fracture mechanism, as demonstrated, among others, by Yamane et al. (2020).

The rolling methods which are analysed in this study are shown in Fig. 1. Method A (Fig. 1a) involves the use of two flat wedges. Method B (Fig. 1b) uses wedges mounted on two rolls. In Method C (Fig. 1c) one roll and one concave tool are used. Method D (Fig. 1d) uses two concave wedges. Also, it is worth noting that Methods C and D have not been analysed in previous studies. This is remarkable given that methods with similar kinematics and tool geometries are used in other areas of manufacturing. Darshith et al. (2014) describe thread rolling methods, including planetary rolling which – in terms of kinematics – is similar to Method C. Miłek (2012) presents a tube end reducing method which – in terms of kinematics – is similar to Method D described in this paper.

2. Research method

Numerical simulations were performed to obtain parameters describing the material's susceptibility to cracking in different CWR methods. The analysed CWR methods were modelled by the finite element method using Simufact Forming 16. The simulations provided data about stresses and strains. Numerical results were then used to determine the material's susceptibility to fracture in different CWR methods. This was done using popular failure criteria. The same boundary conditions and process parameters were used in applied in all analysed rolling methods. In addition, for Methods A, C and D, cases with one moving tool and two moving tools were considered. The methods with one moving tool are marked by 1, while those with two moving tools are marked by 2. In Method B always two tools are moving.

2.1. Fracture criterion used for cracking prediction

The probability of material fracture in the analysed CWR methods was predicted by comparing obtained values of the fracture criterion developed by Pater et al. (2020a). This hybrid fracture criterion is described by the damage function f_{CWR}:

$$f_{CWR} = \int_0^{\varepsilon_f} \left[(1-\Phi)\frac{\sqrt{3}}{2}\frac{\sigma_1-\sigma_3}{\sigma_i} + \Phi\frac{\sigma_1}{\sigma_i} \right] d\varepsilon, \tag{1}$$

where

$$\left\{ \begin{array}{c} \Phi = 0 \text{for} \eta \le 0, \\ \Phi = 3\eta \text{for} 0 < \eta \le 0.333, \\ \Phi = 1 \text{for} \eta > 0.333. \end{array} \right\} \tag{2}$$

σ_i - effective stress, MPa; σ_1 - maximum principal stress, MPa; σ_3 - minimum principal stress, MPa; η - stress triaxiality; ε - effective strain.

According to this criterion, material fracture occurs when the damage function reaches the critical value. This condition is described by the

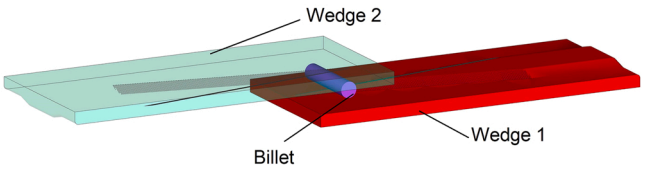

Fig. 2. Numerical model of cross wedge rolling according to Method A, designed in Simufact.Forming.

following relationship:

$$f_{CWR} \geq f_{critical}. \tag{3}$$

The critical damage function $f_{critical}$ is calculated via calibration tests. By definition, these tests must accurately reproduce the state of stress and strain occurring in the real process. Bulzak et al. (2020) used a rotary compression (RC) test for R260 steel to determine the limit damage function. This test consists of using a disc that is compressed between flat plates. The initiation of fracture is determined based on a distance travelled by the rotating disc until the occurrence of a crack. The test is then simulated by FEM. FEM results are used to determine the critical damage function $f_{critical}$ for the experimental distance travelled by the disc until crack occurrence. A similar test was also used by Cheng et al. (2021), who modified the disc geometry. The discs used by Pater et al. (2020a), (2020b), (2020c), (2021) were regular cylinders, while the discs used by Cheng et al. had chamfered edges to reduce the size of cavities that would form on the end faces of the discs during the test. To date no comparative studies have been conducted to determine which disc type reproduces most accurately the real CWR process conditions. Pater et al. (2021) also proposed a test for determining the critical damage function $f_{critical}$ in skew rolling. This test consisted of rolling conical specimens and made it possible to determine the limit reduction causing material fracture. A FE simulation of this test makes it possible to determine the critical value of the damage function $f_{critical}$. The critical value is calculated based on the FEM distribution of the damage function for the crack initiation point that was determined via experimental testing.

The use of the above tests is a new approach to the problem of material fracture prediction in cross wedge and skew rolling processes. Pater et al. (2020c) found that although the stresses in cross wedge rolling and rotary compression test were in high agreement in terms of the stress triaxiality parameter η, there was some discrepancy regarding the Lode angle parameter θ in CWR and RC. In light of the above, in this study, the critical value of the damage function $f_{critical}$ was calculated in a different way. The critical damage function value $f_{critical}$ described by Eq. (1) was determined via a cross wedge rolling process conducted with a smaller reduction. In this way it is possible to ensure that identical rolling conditions will be maintained. A limitation of this test is that the maximum value of the critical damage function $f_{critical}$ must be determined accurately. On the other hand, it is almost certain that no fracture will occur if the damage function values are lower than the critical damage function $f_{critical}$.

2.2. Numerical modelling by the finite element method (FEM)

Numerical models of the analysed rolling methods were designed in accordance with the schematic designs shown in Fig. 1. An example of a numerical model designed for Method A is shown in Fig. 2. All tools had a forming angle of $\alpha = 15°$, a tool angle of $\beta = 10°$, as well as the same length and width of the forming and sizing zones. Other parameters resulting from differences in the kinematics of the analysed methods are shown in Fig. 3. In Method 1 A the tool had a velocity of 300 mm/s. In Method 2 A the tools had a velocity of 150 mm/s. In Method B the rotational speed was set to 8.4 rpm so that the roll had a tangential velocity of 150 mm/s. In Method 1 C the roll was rotated with a speed of 16.8 rpm, as a result of which the roll moved with a tangential velocity of 300 mm/s. In Method 2 C in order to ensure that the tools had a tangential velocity of 150 mm/s, the roll was rotated with a speed of 8.4 rpm while the concave segment with a speed of 7.45 rpm. In Method 1D the concave wedge moved with a velocity of 300 mm/s along the

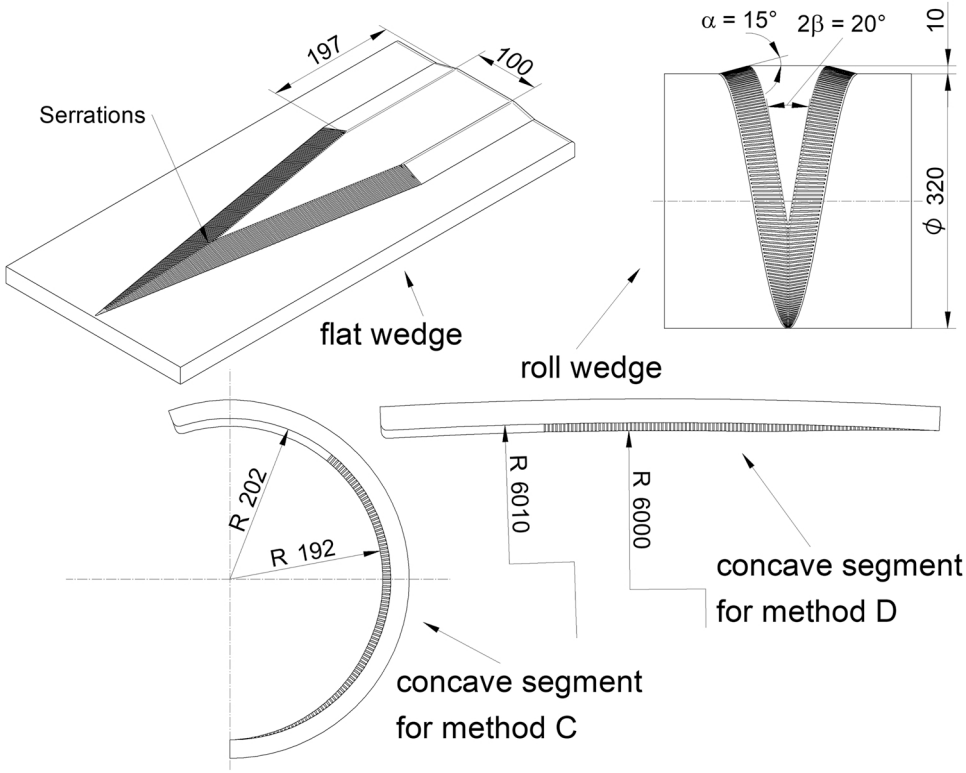

Fig. 3. Parameters of the tools used in FE simulations.

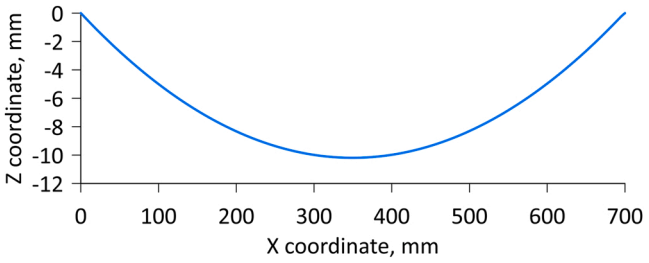

Fig. 4. Trajectory of the concave wedge.

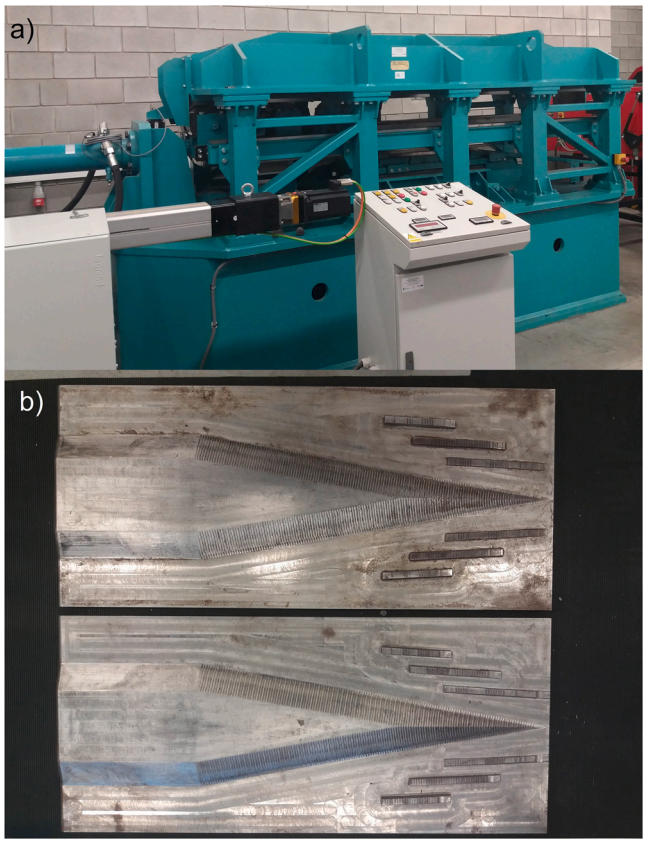

Fig. 5. Equipment used in the experiments: a) flat tool rolling mill, b) wedge tools.

trajectory shown in Fig. 4. Two concave wedges moved along the same trajectory (Fig. 4), each with a velocity of 150 mm/s. These speeds were twice as low for the methods with two moving tools. In effect, it was possible to make the analysed methods similar in terms of process duration, strain rate in the axial zone, and temperature drop during rolling. The initial dimensions of the workpiece were $d_0 = 33$ and $l_0 = 160$ mm. Necking with a diameter of $d_1 = 22$ mm was rolled on the workpiece. The reduction ratio was $\delta = d_0/d_1 = 1.5$. The workpiece material was C45 steel, the rheological properties of which are described by the following equation:

$$\sigma_F = 1521.3 \bullet e^{-0.0027T} \bullet \varepsilon^{-0.1265} \bullet e^{-0.05958/\varepsilon} \bullet \dot{\varepsilon}^{0.1454}, \quad (4)$$

where σ_F - flow stress, ε - effective strain, $\dot{\varepsilon}$ - effective strain rate, T – temperature.

The rolling process was conducted at 1150 °C. The temperature of the tools was maintained constant at 50 °C. Thermal contact in this process was described by a workpiece-tool heat exchange coefficient of 10 kW/m^{2}K and a workpiece-environment heat exchange coefficient of

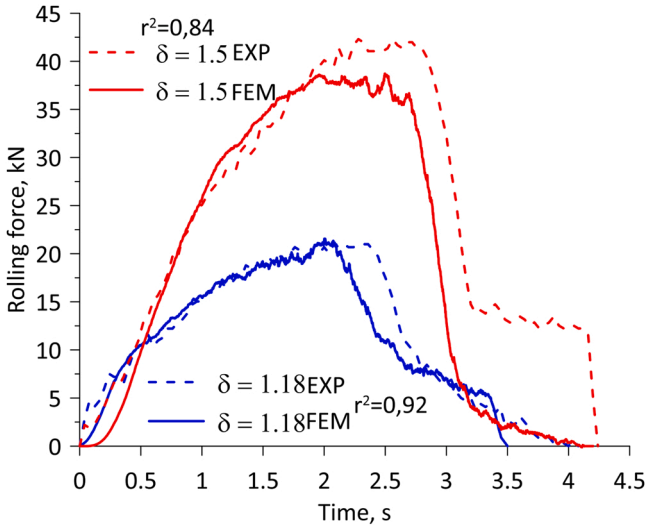

Fig. 6. Variations in the rolling force, used for numerical model validation.

0.05 kW/m^{2}K. Mechanical contact was described by constant friction, and the friction factor was made equal to 0.8. It was assumed that 90% of deformation work would be converted into heat.

In order determine the critical damage function $f_{critical,}$ the case of rolling a billet with initial dimensions of $d_0 = 26$ and $l_0 = 228$ mm was also simulated. Necking with a diameter of $d_1 = 22$ mm was rolled on the workpiece. The reduction ratio was $\delta = d_0/d_1 = 1.18$.

2.3. Experimental

Experiments were carried out on a flat-wedge rolling mill using the same flat tools as in the simulation of Method 1 A. The aim of the experiments was to validate the developed numerical model. The numerical model was validated through the example of Method 1 A. This rolling method was selected for numerical model verification due to the availability of a rolling mill for conducting this type of rolling. In practice, it is also possible to verify Method B because there exist two-roll rolling mills. However, it is impossible to validate Methods C and D because there are no rolling mills that would allow the realization of these rolling methods. The rolling mill and tool set used in the experiments are shown in Fig. 5. The experimental conditions were the same as those adopted in the numerical simulations. The material was preheated in an electric chamber furnace before the rolling process.

2.4. Validation of the numerical model

The numerical model was validated by qualitative and quantitative assessment of experimental and FEM rolling forces, as shown in Fig. 6. For the case of $\delta = d_0/d_1 = 1.5$, the FEM and experimental forces show agreement. This agreement was assessed quantitatively based on the coefficient of determination r^2. For $\delta = d_0/d_1 = 1.5$, the coefficient of determination is $r^2 = 0.84$. The obtained r^2 value shows high agreement between the FEM and experimental results. The agreement between the numerical and experimental results is higher for an early stage of the rolling process, while a clear discrepancy between the results can be observed with respect to a later stage of the rolling process, in which the experimental rolling force values are higher. This situation can be explained by the fact that a crack occurred in the workpiece during the experiment. The internal crack caused ovalization of the cross section of the workpiece, which led to an increase in the rolling force. In the numerical model, the workpiece does not fracture (the workpiece is a continuous medium) and therefore the FEM rolling force is lower.

The FEM model was also validated for the case of $\delta = d_0/d_1 = 1.18$, in which no fracture occurred. This case was also used to determine the

Fig. 7. Samples rolled in the experiments: a) sample rolled at $\delta = 1.5$; b) sample rolled at $\delta = 1.18$.

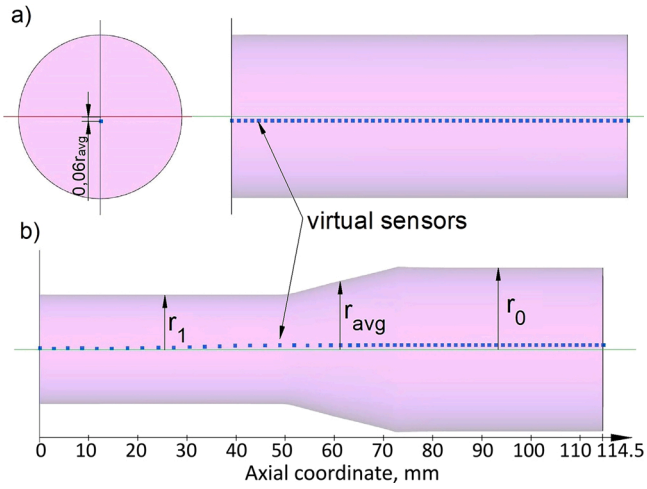

Fig. 8. Location of virtual sensors for measuring stress, strain and damage function: a) workpiece, b) rolled part.

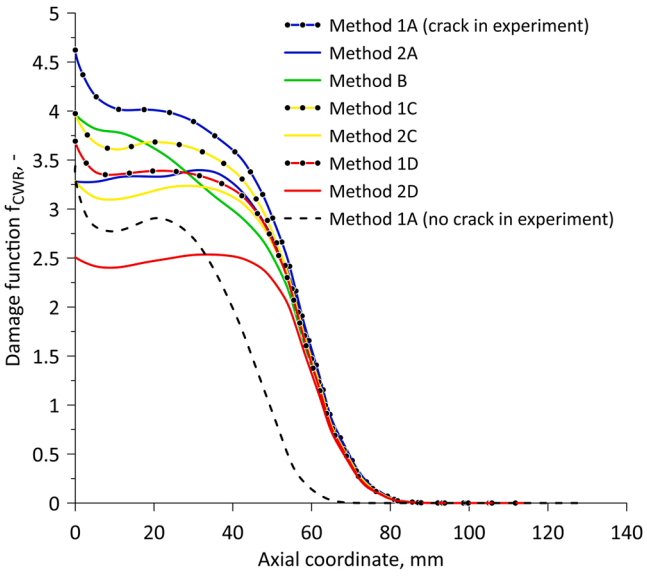

Fig. 9. Distribution of the damage function in the axis of the workpiece, for different rolling methods.

critical value of the damage function $f_{critical}$. For this case, the coefficient of determination r^2 is equal to 0.92. The obtained r^2 value shows high agreement between the FEM and experimental results. The high value of r^2 confirms that the discrepancies between the FEM and experimental forces obtained at $\delta = d_0/d_1 = 1.5$ result from material separation, a phenomenon which does not occur in FEM but leads to the rolling force increase in the experiment. The results of numerical model validation make it possible to claim that the developed numerical model shows high agreement with the experimental cross wedge rolling process.

3. Results

Fig. 7 shows rolled samples. Half of each sample was milled to expose cracks. The sample rolled with a reduction of $\delta = 1.5$ has a visible crack in the axial zone. In contrast, the sample rolled with a reduction of $\delta = 1.18$ has no internal cracks.

The damage function f_{CWR} for the analysed cases was measured with sensors, whose initial location is shown in Fig. 8a. The ultimate location of these sensors after the rolling process is shown in Fig. 8b. The initial location of the sensors was shifted relative to the axis of the workpiece by a value of $0.06r_{avg}$. The r_{avg} value was determined based on the data in Fig. 8b. The shifting of the sensors by $0.06r_{avg}$ relative to the axis of the workpiece was prompted by results obtained by Yamane et al. (2020), whose study showed that fracture in 2-rolling processes conducted with two tools would initiate in a region that was shifted relative to the axis of the workpiece.

The values of the damage function f_{CWR} obtained at the measuring points (Fig. 8) are shown in Fig. 9. It can be seen that the damage function depends on both the applied rolling method and the number of moving tools. The highest damage function value is obtained when rolling by Method 1A, whereas the smallest damage function value is obtained for Method 2D. For all considered rolling methods, the damage function values are lower when rolling is conducted with two moving tools. Among the rolling methods with one moving tools, Method 1D is the most advantageous, while Method 1A is the least advantageous. Considering the methods with two moving tools, Method B is the least advantageous, while method 2D is the most advantageous.

For the rolling methods with one moving tool it can be observed that the peak value of the damage function is located where the wedge begins to cut into the workpiece. The most undesired process conditions conducive to internal crack formation can be observed at an early stage of the rolling process conducted with one moving tool. As for the rolling methods with two moving tools, the distribution of damage function values is more uniform. The only exception is Method B, in which the damage function value decreases in the axis of the workpiece. Considering the experimental results (Method 1 A at $\delta = 1.5$ with fracture and Method 1 A at $\delta = 1.18$ without fracture) and the damage function values determined for these rolling cases, it can be concluded that in Method 2D material fracture will not occur as long as the rolling conditions are the same as those applied in the FEM analysis.

4. Discussion and analysis of the results

The results indicate that the damage function value depends on both the rolling method and the number of moving tools. For a more detailed analysis of this dependency, the relationship between the applied rolling method and the state of stress and strain was also investigated.

4.1. Stress triaxiality and Lode angle parameter

Assuming that the studied material is isotropic, the stress state can be determined via three invariants of the stress tensor:

$$p = -\sigma_m = -\frac{1}{3}(\sigma_1 + \sigma_2 + \sigma_3), \tag{5}$$

$$q = \sigma_i = \sqrt{\frac{1}{2}\left[(\sigma_1 - \sigma_2)^2 + (\sigma_2 - \sigma_3)^2 + (\sigma_1 - \sigma_3)^2\right]}, \tag{6}$$

$$r = \left[\frac{27}{2}(\sigma_1 - \sigma_m)(\sigma_2 - \sigma_m)(\sigma_3 - \sigma_m)\right]^{\frac{1}{3}}, \tag{7}$$

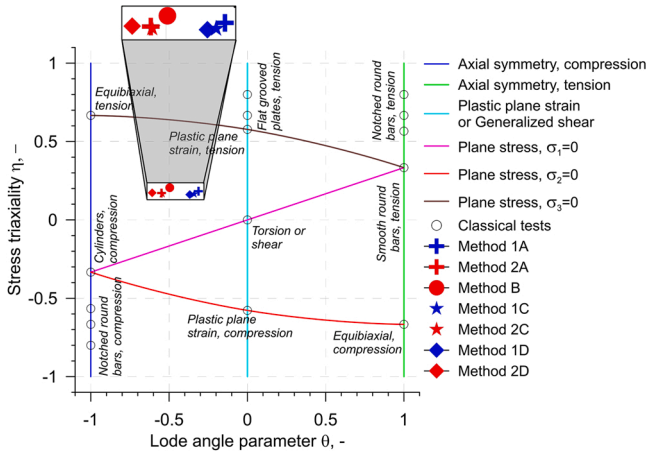

Fig. 10. Stress state in θ-η plane for different variants of cross wedge rolling.

where σ_1, σ_2, σ_3 are the principal stresses, σ_m is the mean stress, σ_i is the effective stress.

Recent studies by Ganjiani (2020) and Kiran et al. (2014) have shown that material fracture in metal forming processes depends on two stress invariants: the stress triaxiality η and the Lode angle parameter θ described by the following equations:

$$\eta = \frac{-p}{q} = \frac{\sigma_m}{\sigma_i}, \tag{8}$$

$$\theta = 1 - \frac{2}{\pi} arccos\left[\left(\frac{r}{q}\right)^3\right]. \tag{9}$$

Since both the stress triaxiality η and the Lode angle parameter θ change their values during the rolling process, their average values as measured by the sensors located as shown in Fig. 8 were calculated using the following relationships:

$$\eta_{av} = \frac{1}{\varepsilon}\int_0^{\varepsilon} \eta \quad d\varepsilon, \tag{10}$$

$$\theta_{av} = \frac{1}{\varepsilon}\int_0^{\varepsilon} \theta \quad d\varepsilon. \tag{11}$$

The average values η_{av} and θ_{av} are shown in a η-θ plane (Fig. 10), along with the values of these parameters obtained with standard tests and specimens for material fracture testing.

The stress triaxiality values are similar for all analysed rolling methods, the only exception being Method B in which the stress triaxiality value is slightly higher. The stress triaxiality values demonstrate that the fracture mechanism is the same for all rolling methods. According to Pater et al. (2020a), when the stress triaxiality ranges $0 < \eta < 0.333$, material fracture can be a result of both void nucleation, growth and coalescence, as well as shear fracture.

Summing up, the rolling method has no significant effect on the CWR fracture mechanism. The Lode angle parameter θ clearly depends on the applied rolling method. For the rolling methods with two moving tools, the absolute values of the Lode angle parameter θ are higher than those obtained when rolling was conducted with only one moving tool. The value of the Lode angle parameter θ obtained by rolling with two rolls is between the values obtained when CWR was performed with one and two moving tools. Regardless of the number of moving tools, the highest absolute values of the Lode angle parameter θ were obtained for Method D. The lowest absolute value of the Lode angle parameter θ (−0.31) was obtained for Method 1 A, while the highest absolute value of θ (−0.6) was obtained for Method 2D.

The relationship between the Lode angular parameter θ and material fracture is explained by means of a fracture plane in the coordinates θ, η,

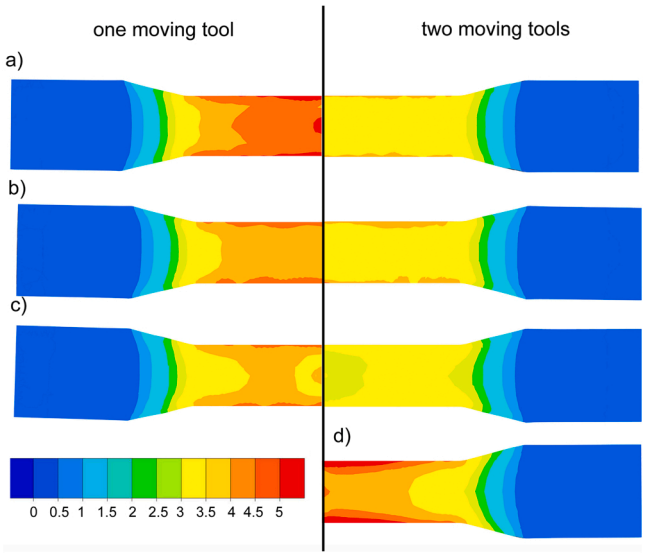

Fig. 11. Distribution of strains for different rolling methods: (a) flat wedges – Method A, (b) roll wedge-concave segment – Method C (c) two concave wedges – Method D (d) roll wedge – Method B.

ε_f for C45 steel developed by Bai et al. (2009). According to Bai et al. (2009), an increase in the absolute value of the Lode angle parameter θ leads to an increase in the plastic strain ε_f (critical strain) causing material fracture. In short, in Method 2D the strain value must be the highest for the material fracture to occur, whereas in Method 1 A fracture occurs when the strain is the lowest.

4.2. Strain state and strain rate

The results of stress demonstrate that the material's susceptibility to cracking in cross wedge rolling depends on the strain value. Therefore, it is also justified to investigate the relationship between strain and rolling method. Fig. 11 shows the distribution of strains obtained via numerical modelling.

One can observe clear differences in the values and distributions of plastic strains depending on the applied rolling method. The strain values are significantly lower for the methods with two moving tools than those obtained for the same methods with one moving tool. In the methods with two moving tools the strains are distributed in a layer-like fashion, i.e. the highest strains are located at the surface and their values gradually decrease with decreasing the distance from the axis of the workpiece (Methods 2A, B and 2C). The only exception is Method 2D in which the strain distribution is not layer-like. In the methods with one moving tool the highest strains are also located on the surface of the workpiece, but their distribution is not so evidently layer-like as is the case with the methods using two moving tools.

For Methods 2A, 2C and 2D the strains have the most uniform distribution, while the most non-uniform strain distribution is obtained for Method B. The highest strain ($\varepsilon_i = 5$) in the axial region of the workpiece is obtained for Method 1A. The lowest strains ($\varepsilon_i = 2.5 \div 5.5$) in the axial region of the workpiece are obtained when rolling is performed by Method 2D. The extreme values of both the damage function and the Lode angle parameter θ are also obtained for these rolling methods. Regarding Method 1A for the smallest value of the Lode angle parameter θ (−0.31), fracture occurs when the strain ε_f presents the lowest value for all analysed methods. It is undesired that the highest strain ($\varepsilon_i = 5$) is obtained for this rolling method. On the other hand, in Method 2D for the highest value of the Lode angle parameter θ (−0.6), the obtained value of the strain ε_f is the highest out of the strain values found for all analysed methods. In Method 2D the high value of the Lode angle parameter θ (−0.6) and the low plastic strain value are very favourable

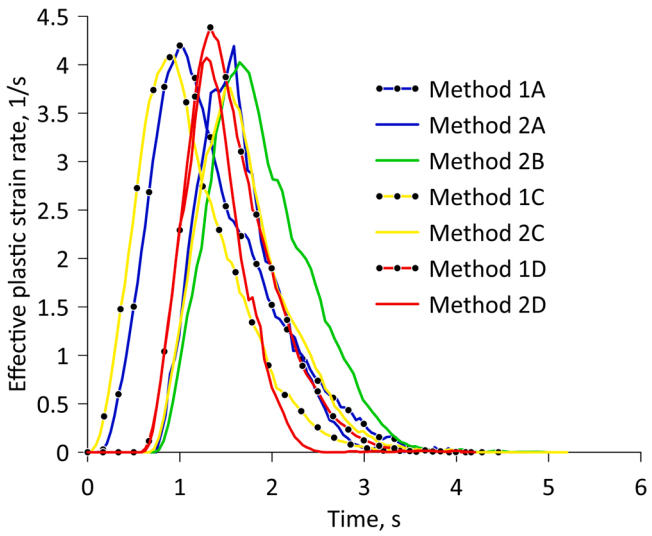

Fig. 12. Effective plastic strain vs. time, for the analysed rolling methods.

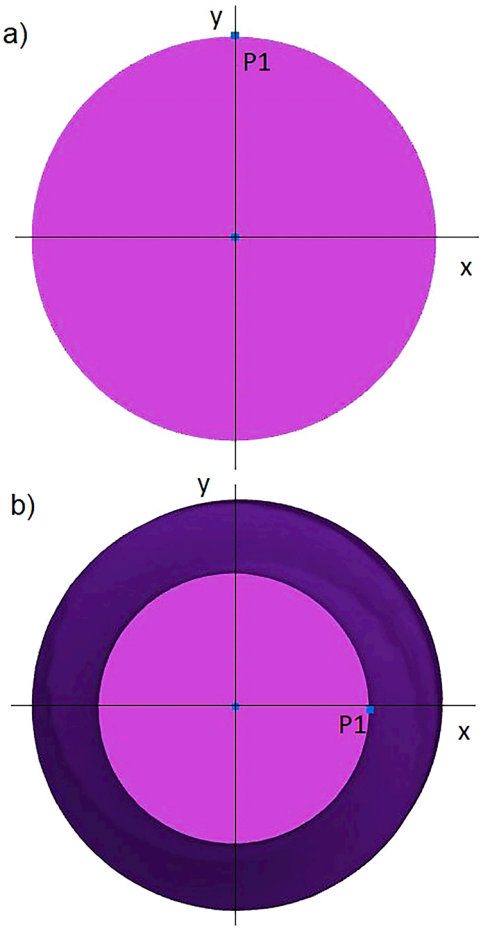

Fig. 13. Location of point P1: a) start of the process, b) end of the process.

and thus material fracture is the least probable.

Results obtained by Marcadet et al. (2015) demonstrate that material fracture also depends on the strain rate. According to the plane of fracture in the coordinates θ, η, ε_f by Marcadet et al. (2015), an increase in the strain rate also leads to an increase in the strain ε_f (critical strain) causing material fracture. Fig. 12 shows the distribution of strain rate in the analysed rolling process. The strain rate was measured with the first of the virtual sensors shown in Fig. 8. The first virtual sensor was located where the axial coordinate was equal to 0 mm. The results demonstrate that the strain rate value obtained for the applied boundary conditions is the same for all analysed rolling methods. The rolling method type has no significant effect on the strain rate. A comparison of the results obtained in this study with the results obtained by Marcadet et al. (2015) reveals that the rolling method has no effect on the strain rate and thus has no effect on the strain ε_f (critical strain) causing material fracture. As a result, all analysed rolling methods can be examined considering one plane of fracture and omitting the impact of strain rate.

4.3. Metal flow pattern

In CWR strains greatly depend on the reduction δ. In this study its value was set to 1.5 in all analysed cases. Given that the reduction value was the same in all CWR cases, the differences in strain should be attributed to different metal flow patterns. To examine the metal flow pattern in individual CWR methods, a point P1 is marked on the circumference of the workpiece (Fig. 13), and the point's trajectories for individual rolling methods are plotted in Fig. 14. An analysis of the trajectories of point P1 in Fig. 14 reveals that cross-sectional ovalization is higher when CWR is conducted with one moving tool. For the rolling methods with one or two moving tools, the trajectory of point P1 begins to change with the second revolution of the workpiece. The degree of cross-sectional ovalization was defined by measuring the maximum distance between the point P1 trajectory and the workpiece centre of rotation Δr after one complete revolution of the workpiece.

Results of the parameter Δr are given in Table 1. An increase in Δr indicates greater ovalization of the cross section of the workpiece during rolling. It can be observed that the cross-sectional ovalization is higher when rolling is conducted with one moving tool, rather than when two moving tools are used. Among the analysed rolling methods, the greatest workpiece cross section ovalization can be observed for Method 1A, while the lowest for Method 2D. The value of Δr corresponds to the strain values shown in Fig. 12. With higher values of Δr, the cross-sectional ovalization is higher, which results in higher strains. On the other hand, when the values of this parameter are lower, the strains are lower too. This is due to the fact that with larger cross-sectional ovalization, additional redundant strains are generated when removing the ovalization. In addition, it is worth noting that in the case of CWR methods with one moving tools, the workpiece must perform more than 2 revolutions in order to achieve the assumed diameter of $d_1 = 22$ mm. As for the methods using two moving tools, the workpiece must complete more than 1.5 revolutions to achieve the required diameter.

4.4. Force conditions

The results reported in the previous section indicate that the degree of ovalization of the cross section of the workpiece, as well as the change in the strain value induced by this ovalization are dependent on the tool geometry (depending on the rolling method applied) and process kinematics (depending on the number of moving tools). The system of forces occurring in cross wedge rolling (Fig. 15) also promotes ovalization of the cross section of the workpiece. Here, the degree of ovalization will depend on the tangential force F_x causing stretching of the cross section of the workpiece. The tensile stress in the central region of the workpiece and the shear stress will also depend on the tangential force F_x. Zhou et al. (2020a), (2020b) and Pater et al. (2020a), (2020b), who are the authors of two fracture criteria for the CWR process, assume that material fracture in CWR primarily depends on the tensile and shear stress. Hence, it seems reasonable to analyse the values of the tangential force F_x obtained in the studied CWR cases.

Fig. 16 shows the tangential force F_x in the analysed rolling methods. It can be observed that the values of the tangential force for the CWR methods with two moving tools are not lower than those obtained for the CWR methods with one moving tool. An opposite trend can only be

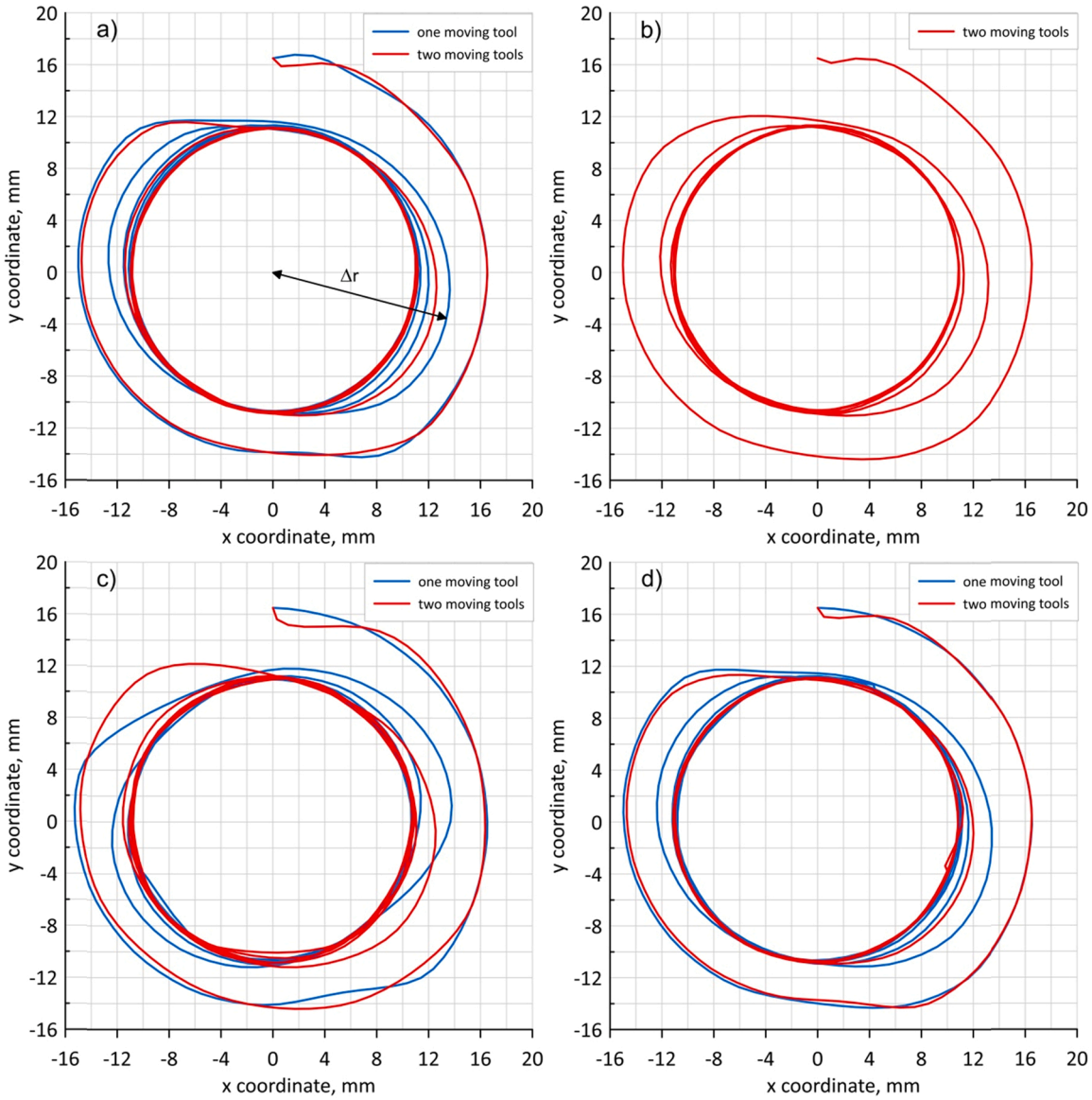

Fig. 14. Point P1 trajectories for different rolling methods: a) flat wedges – Method A, b) roll wedge – Method B, c) roll wedge-concave segment – Method C, d) two concave wedges – Method D.

Table 1
Maximum distance between the point P1 trajectory and the centre of rotation of the workpiece Δr during the second revolution of the tools.

Method	Flat wedges – Method A	Roll wedge – Method B	Roll wedge-concave segment – Method C	Two concave wedges – Method D
One moving tool	13.57 mm	–	13.42 mm	13.27 mm
Two moving tools	12.50 mm	12.96 mm	12.35 mm	11.80 mm

observed for Method 2C, where the tangential force is higher when rolling is conducted with two moving tools. Regarding the methods with one moving tool, the highest tangential force is obtained for Method 1A (flat wedges), while the lowest force values are observed for Method C (roll wedge-concave segment). As for the CWR methods with two moving tools, the highest tangential force is also obtained for Method 2A (flat wedges), while the lowest values of this force are obtained for Method B where rolling is conducted with two rotating rolls. In Method 2A the tangential force F_x decreased by only 4%, in Method 1C it decreased by 3.4%, while in Method 2D the force decreased by 11.6%. All in all, it can be concluded that the use of two moving tools reduces the tangential rolling force in Methods 2A and 2D. The relationship between the force and the number of moving tools is most evident for Method 1D and Method 2D. According to data in Fig. 15, the tangential force F_x can affect the tensile stress σ_t and the shear stressτ.

4.5. State of stress

The tensile stress σ_t and the maximum shear stress $\tau_{max} = (\sigma_1\text{-}\sigma_3)/2$ were measured with the first virtual sensor, as shown in Fig. 8. This virtual sensor was located where the axial coordinate equalled 0 mm. Fig. 17 shows the distribution of tensile stress σ_t. Fig. 18 shows the distribution of maximum shear stress τ_{max}.

The results demonstrate that the tensile stress in the central area of the workpiece depends on the number of moving tools. The tensile stress is definitely higher when rolling is conducted with one moving tool. The highest tensile stresses are observed for Method 1A, while the lowest

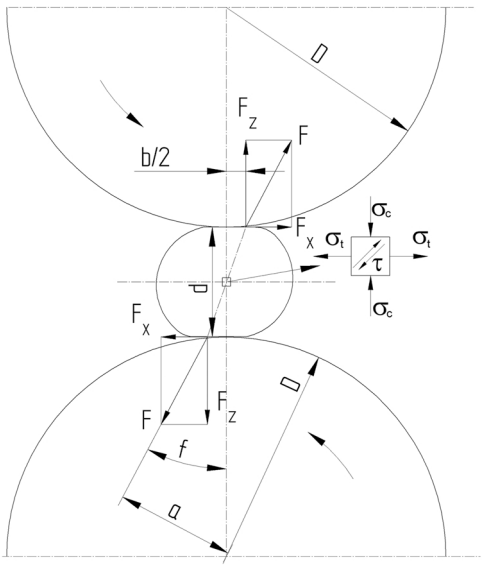

Fig. 15. Forces in cross wedge rolling.

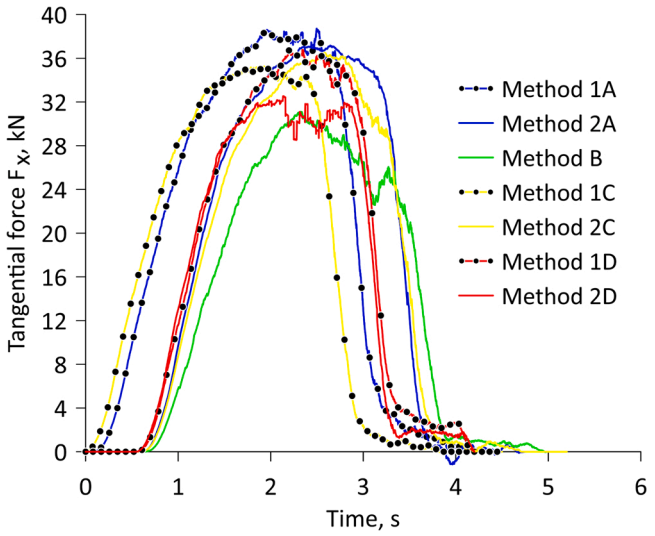

Fig. 16. Tangential force F_x versus time, for the analysed rolling methods.

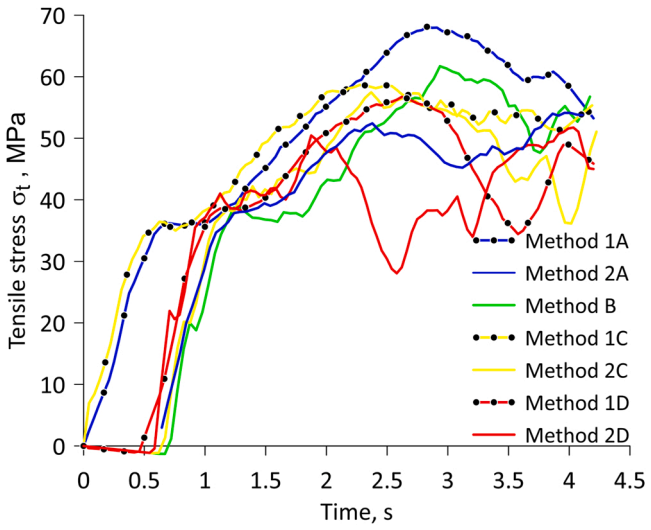

Fig. 17. Tensile stress σ_t versus time, for the analysed rolling methods.

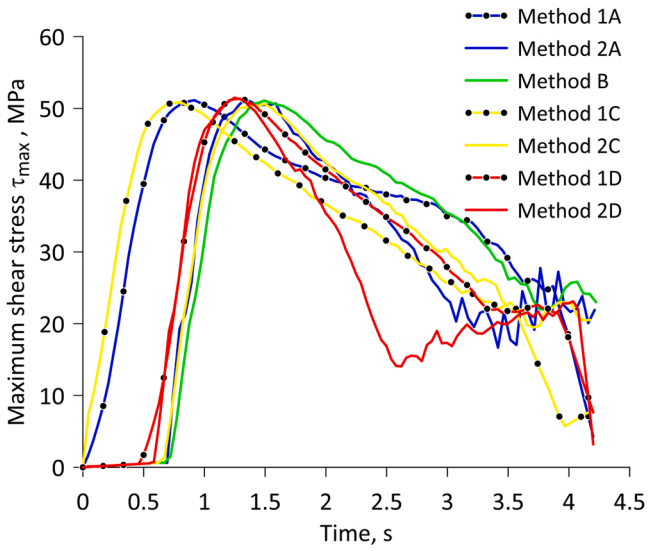

Fig. 18. Maximum shear stress τ_{max} versus time, for the analysed rolling methods.

tensile stresses are observed for Method 1D. A reduction in the number of moving tools leads to an increase in the maximum tensile stress by 20.6% for Method A, 4.8% for Method C and 9.7% for Method D.

A similar pattern of changes in the maximum shear stress τ_{max} can be observed for all analysed rolling methods. At an early stage of the rolling process the maximum shear stress τ_{max} quickly reaches the maximum and gradually decreases to reach the minimum toward the end of the rolling process. For all rolling methods, the maximum shear stress τ_{max} is 51 MPa. Having reached the highest value, the maximum shear stress τ_{max} begins to decrease gradually, which is observed for all rolling methods. With Methods A and D, the maximum shear stress τ_{max} decreases faster when rolling is conducted with two moving tools. Regarding Method C, the maximum shear stress τ_{max} decreases at a similar rate, and the decrease rate does not depend on the number of moving tools.

The curves (Figs. 17 and 18) showing the changes in the maximum shear stress τ_{max} and tensile stress σ_t do not unequivocally indicate which rolling method causes the highest material effort due to these stresses. This results from a rather irregular pattern of changes in the stresses during rolling, which makes it difficult to precisely determine material effort. In many cases, material separation (crack) occurs after exceeding the limit strength, e.g. in a uniaxial tensile test. Results of the rotary compression test obtained by Pater et al. (2020c) demonstrate that material fracture does not occur after reaching the maximum stress value but is initiated after some time, after the stresses acting on the workpiece have completed the required amount of deformation work. Fig. 19 shows a plot illustrating changes in the tensile stress σ_t and the maximum shear stress τ_{max} in the rotary compression test. It is clear from the plot that material fracture due to the Mannesmann effect occurs after a certain period of time when the stresses acting on the workpiece have completed the required amount of deformation work. It is also evident from this plot that the material fracture occurs at lower stress values than those measured at the beginning of the test. Therefore, it is assumed that the stress value is not as important as the total value of stresses acting on the workpiece in the rolling process.

In light of the above, it was decided to calculate the area under the curves shown in Fig. 17 and Fig. 18 in order to sum the stresses induced on the workpiece throughout the rolling process. Obtained curve integration results are listed in Table 2. The total tensile as well as shear stresses are higher for the methods using one moving tool. Specifically,

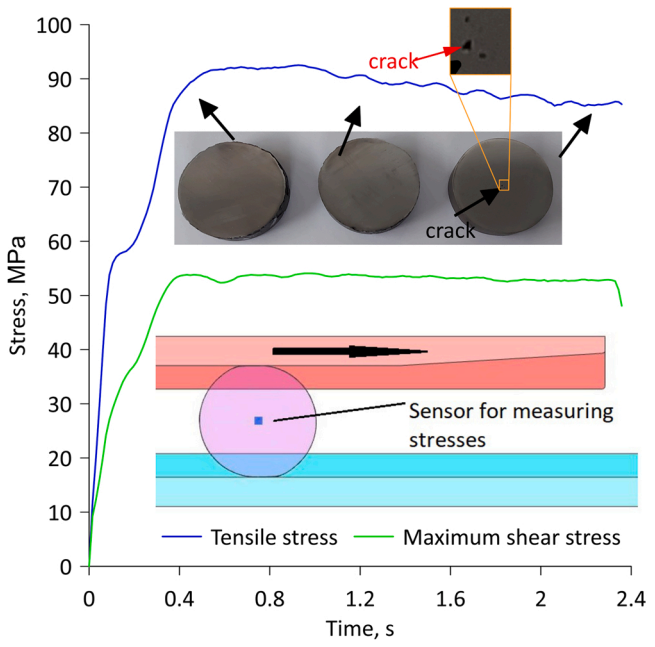

Fig. 19. Variations in tensile stress σ_t and maximum shear stress τ_{max} in rotary compression test.

both the total tensile stress and the total shear stress are the lowest for Method 2D, whereas these values are the highest for Method 1A. The total tensile stress and the total maximum shear stress indicate that the lowest material effort occurs when rolling by Method 2D while the highest material effort will occur when the rolling process is conducted by Method 1A. Table 2 also shows in brackets the percentages of individual components making up the total tensile and shear stress values. The results show that Methods 1A and 1C induce the highest percentage of tensile stress, while the lowest percentage of tensile stress is observed for Method 2D. The percentage of tensile stress is also slightly lower when rolling with two moving tools.

4.6. *Mechanism of increase in ovalization of the cross section of a rolled forging*

The results presented above indicate that ovalization of the cross-section of the rolled product depends on the rolling method and the number of moving tools. It was also shown that an increase in section ovalization during rolling results in an increase in the values of parameters determining the value of fracture criterion, i.e. effective strain ε_i, tensile stress σ_t and maximum shear stress τ_{max}. The increase of the above-mentioned parameters is a result of the fact that a forging that has a larger ovalization of the cross-section requires a larger forming path in order to remove this ovalization. The removal of cross-sectional ovalization leads to an increase in redundant strain, which translates into greater reduced effective strain ε_i. In addition, material shaped over a longer distance is subjected to increased stresses during removal of excessive ovalization, which in turn leads to increased tensile stress σ_t and maximum shear stress τ_{max}.

The forging is rotated by frictional forces in the tool contact zone. When the movement is performed by one tool, the instantaneous centre of rotation ICR (velocity is equal to 0 mm/s) of the forging is in the contact zone with the fixed tool (Fig. 20a), while when the movement is performed by both tools, the centre of rotation CR of the forging is in its central zone (Fig. 20b). When considering the rolling process at a given moment in time, it can be assumed that the forging on the fixed tool remains at rest, and the friction occurring for this pair will have a resting

Table 2
Measure of material effort induced by the tensile stress σ_t and the maximum shear stress τ_{max}.

Method	Flat wedges – method A	Roll wedge – method B	Roll wedge-concave segment – method C	Two concave wedges – method D
Total tensile stress σ_t				
One moving tool	208.4 MPa·s (58.6%)	–	194.8 MPa·s (59.6)	137.4 MPa·s (53.5%)
Two moving tools	155.4 MPa·s (57.4%)	159.8 MPa·s (55.7%)	159.6 MPa·s (57.3)	114.4 MPa·s (52.8%)
Total maximum shear stress τ_{max}				
One moving tool	146.9 MPa·s (41.4%)	–	131.9 MPa·s (40.4%)	119.2 MPa·s (46.5%)
Two moving tools	115.2 MPa·s (42.6%)	127.1 MPa·s (44.3%)	118.8 MPa·s (42.7%)	101.9 MPa·s (47.2%)
Total tensile stress σ_t + total maximum shear stress τ_{max}				
One moving tool	355.3 MPa·s	–	326.7 MPa·s	256.6 MPa·s
Two moving tools	270.6 MPa·s	286.9 MPa·s	278.4 MPa·s	216.3 MPa·s

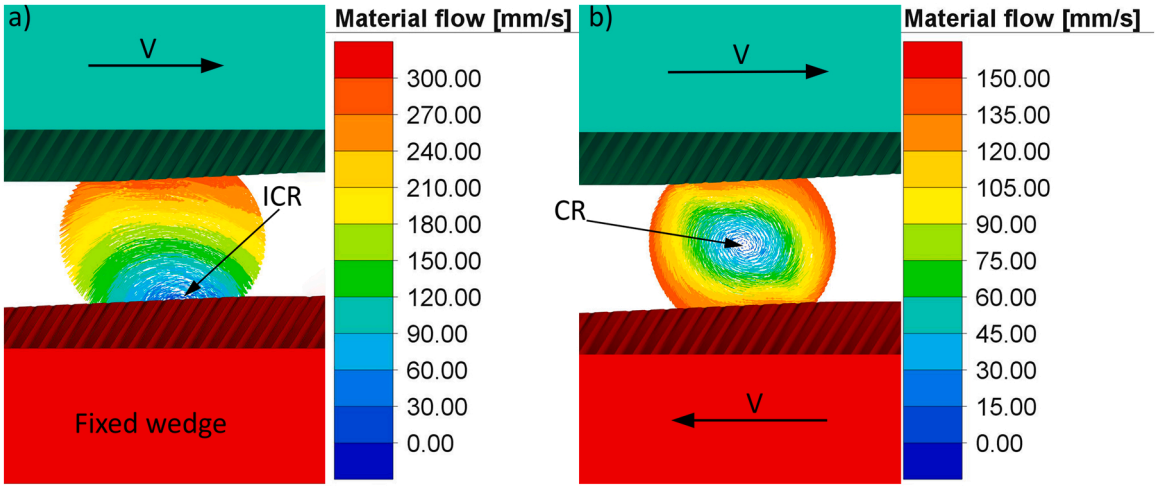

Fig. 20. Flow velocity diagram of the material for: a) one moving tool, b) two moving tools.

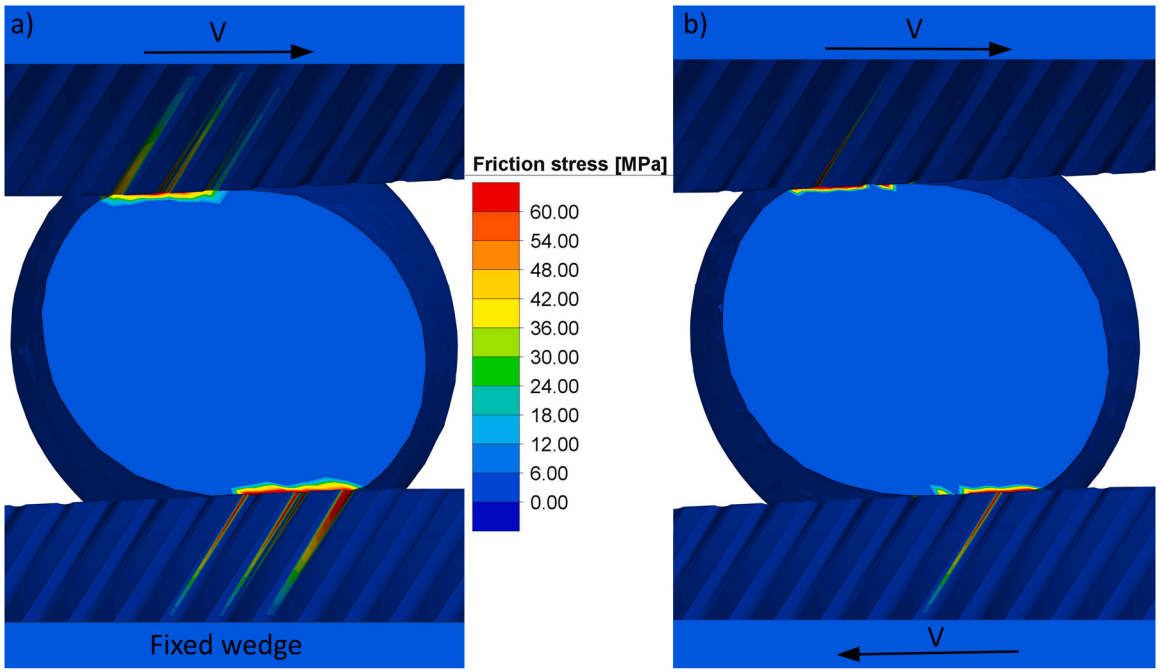

Fig. 21. Friction stress distribution for: a) one moving tool, b) two moving tools.

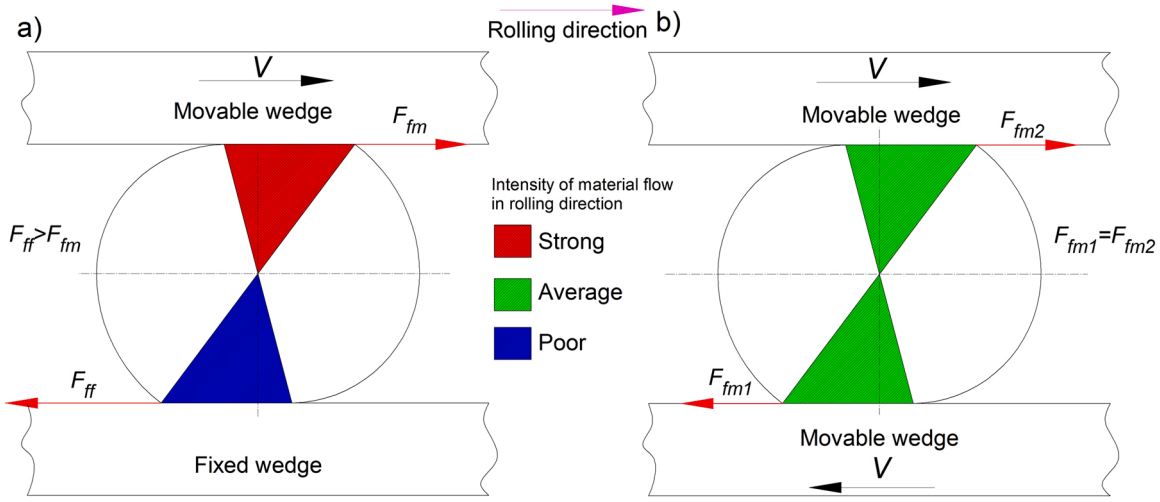

Fig. 22. Mechanism of section ovalization development during: a) one moving tool, b) two moving tools.

(static) character. In the case of contact between the forging and a moving tool, the friction will be of a moving (kinetic) nature. Information presented by Persson et al. (2003), among others, shows that static friction forces are greater than kinetic friction forces.

Fig. 21 shows the distribution of frictional stress determining the value of frictional forces occurring in the contact zone between tools and rolled material. When rolling with a single moving tool, the frictional forces in the tool contact zone will differ from each other as a result of different frictional stress values on individual tools. Thus, the frictional force will be higher on a stationary tool compared to a moving tool. In the case of two moving tools, the frictional forces will be equal, which is confirmed by a similar frictional stress distribution.

The occurrence of different frictional forces on the individual tools favours an increase in ovalization of the cross-section of the forging during rolling. The increase in ovalization is due to the inhibition of material flow on the lower tool by higher friction forces, as a result of which the moving tool causes increased stretching of the cross-section of the rolled forging in the direction of rolling, thus causing an increase in the degree of ovalization of the cross-section of the rolled forging (Fig. 22a). The balanced frictional forces for the method using two moving tools result in a uniform rotation of the forging without the effect of overstretching the cross-section (Fig. 22b).

The tendency of the rolled material to ovalization in the case of concave tools is lower in comparison with, for example, flat tools, because the material during rolling is girdled by the concave surfaces of the tools, which mechanically block excessive flow of material in the direction of rolling and thus limit ovalization of the cross-section of the rolled forging (Fig. 23).

5. Conclusions

A comparison of the cross wedge rolling methods analysed in this study has provided new valuable data about material fracture in this process. The results lead to the following conclusions:

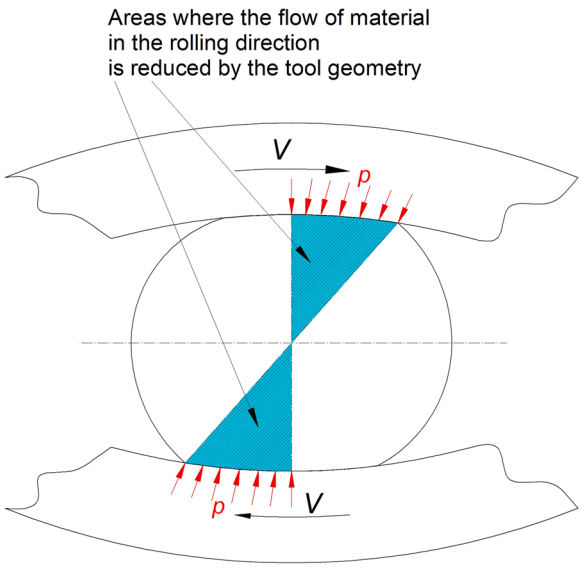

Fig. 23. Locking mechanism of material flow in the rolling direction for concave tools.

- Material fracture in cross wedge rolling was most likely to occur when the rolling process was conducted with one moving flat wedge tool (Method 1A).
- The lowest probability of material fracture was observed when the rolling process was conducted with two moving concave wedges (Method 2D).
- The probability of material fracture was lower when CWR was performed with two moving tools rather than with one moving tool.
- The damage function value differences observed for the analysed rolling methods resulted from different metal flow patterns in these rolling methods, which led to the differences in workpiece cross section opalization in the rolling cases under analysis.

CRediT authorship contribution statement

Tomasz Bulzak: Conceptualization, Methodology, Software, Data curation, Writing – original draft. **Zbigniew Pater**: Validation, Writing – review & editing. **Janusz Tomczak**: Investigation, Resources. **Łukasz Wójcik**: Investigation. **Alberto Murillo-Marrodán**: Visualization, Formal analysis, Writing – review & editing.

Declaration of Competing Interest

The authors declare that they have no known competing financial interests or personal relationships that could have appeared to influence the work reported in this paper.

Acknowledgement

The research was financed in the framework of the project: Development of new rolling technologies for rail axle forgings, No. LIDER/9/0060/L-12/20/NCBR/2021. Total cost of the Project: 1 466 831.25 PLN. The project is financed by the National Centre for Research and Development under the 12th edition of the LIDER Programme.

References

Bai, Y., Teng, X., Wierzbicki, T., 2009. On the application of stress triaxiality formula for plane strain fracture testing. J. Eng. Mater. Technol. 131 (2), 021002 https://doi.org/10.1115/1.3078390.

Bulzak, T., Pater, Z., Tomczak, J., Wójcik, Ł., 2020. A rotary compression test for determining the critical value of the cockcroft–latham criterion for R260 steel. Int. J. Damage Mech. 29 (6), 874–886. https://doi.org/10.1177/1056789519887527.

Carkicrcali, M., Kilicaslan, C., Guden, M., Kiranli, E., Shchukin, V.Ya, Petronko, V.V., 2013. Cross wedge rolling of a TiAl4V (ELI) alloy: the experimental studies and the finite element simulation of the deformation and failure. Int. J. Adv. Manuf. Technol. 65, 1273–1287. https://doi.org/10.1007/s00170-012-4256-3.

Cheng, M., Shi, M.J., Petrenko, V., Wang, R.X., Zhang, S.H., 2021. Novel evaluation method for metal workability during cross wedge rolling process. Adv. Manuf. 9, 473–481. https://doi.org/10.1007/s40436-020-00344-9.

Darshith, S., Ramesh, B.K., Manjunath, S.S., 2014. Comprehensive study of cut and roll threads. IOSR J. Mech. Civ. Eng. 11 (2), 91–96.

Dong, Y., Tagavi, K.A., Lovell, M.R., Deng, Zhi, 2000. Analysis of stress in cross wedge rolling with application to failure. Int. J. Mech. Sci. 42, 1233–1253. https://doi.org/10.1016/S0020-7403(99)00035-1.

Fu, X.P., Dean, T.A., 1993. Past developments, current applications and trends in the cross wedge rolling process. Int. J. Mach. Tools Manuf. 33 (3), 367–400. https://doi.org/10.1016/0890-6955(93)90047-X.

Ganjiani, M., 2020. A damage model for predicting ductile fracture with considering the dependency on stress triaxiality and Lode angle. Eur. J. Mech. A Solids 84, 104048. https://doi.org/10.1016/j.euromechsol.2020.104048.

Huang, X., Wang, B., Zhou, J., Ji, H., Mu, Y., Li, J., 2017. Comparative study of warm and hot cross-wedge rolling: numerical simulation and experimental trial. Int. J. Adv. Manuf. Technol. 92, 3541–3551. https://doi.org/10.1007/s00170-017-0399-6.

Huo, Y., Lin, J., Bai, Q., Wang, B., Tang, X., Ji, H., 2017. Prediction of microstructure and ductile damage of a high-speedrailway axle steel during cross wedge rolling. J. Mat. Process. Technol. 239, 359–369. https://doi.org/10.1016/j.jmatprotec.2016.09.001.

Jia, Z., Zhou, J., Ji, J., Yu, Y., Xiao, C., 2012. Influence of tool parameters on internal voids in cross wedge rolling of aluminums alloy parts. Trans. Nonferrous Met. Soc. 22, 21–26. https://doi.org/10.1016/S1003-6326(12)61678-1.

Jia, Z., Ji, J., Wang, Y., Wei, B., 2020. Influence of die parameters on internal voids during multi-wedge-multi-pass cross-wedge rolling. Int. J. Adv. Manuf. 110, 1295–1304. https://doi.org/10.1007/s00170-020-05897-4.

Kiran, R., Khandelwal, K., 2014. A triaxiality and Lode parameter dependent ductile fracture criterion. Eng. Fract. Mech. 128, 121–138. https://doi.org/10.1016/j.engfracmech.2014.07.010.

Komischke, T., Hora, P., Domani, G., Plamondon, M., Kaufmann, R., 2018. Prediction of crack induced failure phenomena in rolling operations. Procedia Manuf. 15, 176–184. https://doi.org/10.1016/j.promfg.2018.07.192.

Lee, H.W., Lee, G.A., Yoon, D.J., Choi, S., Na, K.H., Hwang, M.Y., 2008. Optimization of design parameters using a response surface method in a cold cross-wedge rolling. J. Mater. Process. Technol. 201, 112–117. https://doi.org/10.1016/j.jmatprotec.2007.11.287.

Li, Q., Lovell, M.R., 2004. The establishment of failure criterion in cross wedge rolling. Int. J. Adv. Manuf. Technol. 24, 180–189. https://doi.org/10.1007/s00170-003-1607-0.

Li, Q., Lovell, M.R., 2008. Cross wedge rolling failure mechanisms and industrial application. Int. J. Adv. Manuf. Technol. 37, 265–278. https://doi.org/10.1007/s00170-007-0979-y.

Li, Q., Lovell, M.R., Slaughter, W., Tagavi, K., 2002. Investigation of internal defects in cross wedge rolling. J. Mater. Process. Technol. 125–126, 248–257. https://doi.org/10.1016/S0924-0136(02)00303-5.

Liu, G., Zhong, Z., Shen, Z., 2014. Influence of reduction distribution on internal defects during cross wedge- rolling process. Procedia Eng. 81, 263–267. https://doi.org/10.1016/j.proeng.2014.09.161.

Marcadet, S.J., Roth, C.C., Erice, B., Mohr, D., 2015. A rate-dependent hosford-coulomb model for predicting ductile fracture at high strain rates. EPJ Web Conf. 94, 01080. https://doi.org/10.1051/epjconf/20159401080.

Miłek, T., 2012. Experimental investigations into one-sided and two-sided bulge forming of steel reducing tubes. Steel Res. Int. 543–546.

Novella, M.F., Ghiotti, A., Bruschi, S., Bariani, P.F., 2014. Modelling of AA6082 ductile damage evolution under hot rolling conditions. Procedia Eng. 81, 221–226. https://doi.org/10.1016/j.proeng.2014.09.154.

Novella, M.F., Ghiotti, A., Bruschi, S., Bariani, P.F., 2015. Ductile damage modeling at elevated temperature applied to the cross wedge rolling of AA6082-T6 bars. J. Mater. Process. Technol. 222, 259–267. https://doi.org/10.1016/j.jmatprotec.2015.01.030.

Pater, Z., Tomczak, J., Bulzak, T., 2020a. Establishment of a new hybrid fracture criterion for cross wedge rolling. Int. J. Mech. Sci. 167, 105274 https://doi.org/10.1016/j.ijmecsci.2019.105274.

Pater, Z., Tomczak, J., Bulzak, T., 2020b. Rapid estimation of ductile crack formation in cross-wedge rolling. J. Mater. Res. Technol. 9 (6), 14360–14371. https://doi.org/10.1016/j.jmrt.2020.10.046.

Pater, Z., Tomczak, J., Bulzak, T., 2020c. Rotary compression as a new calibration test for prediction of a critical damage value. J. Mater. Res. Technol. 9 (3), 5487–5498. https://doi.org/10.1016/j.jmrt.2020.03.074.

Pater, Z., Tomczak, J., Bulzak, T., Wójcik, Ł., Skripalenko, M.M., 2021. Prediction of ductile fracture in skew rolling processes. Int. J. Mach. Tools Manuf. 163 (9), 103706 https://doi.org/10.1016/j.ijmachtools.2021.103706.

Persson, B.N.J., Albohr, O., Mancosu, F., Peveri, V., Samoilov, V.N., Sivebaek, I.M., 2003. On the nature of the static friction, kinetic friction and creep. Wear 254, 835–851. https://doi.org/10.1016/S0043-1648(03)00234-5.

Silva, M.L.N., Pires, G.H., Button, S.T., 2011. Damage evolution during cross wedge rolling of steel DIN 38MnSiVS5. Procedia Eng. 10, 752–757 https://doi.org/10.1016/j.proeng.2011.04.125.

Yamane, K., Shimoda, K., Kuroda, K., Kajikawa, S., Kuboki, T., 2020. A new ductile fracture criterion for skew rolling and its application to evaluate the effect of number

of rolls. J. Mater. Process. Technol. 291, 116989 https://doi.org/10.1016/j.jmatprotec.2020.116989.
Yang, C., Zhang, K., Hu, Z., 2012. Development of central minute cavity in the workpiece of cross wedge rolling. Appl. Mech. Mater. 215–216, 766–770. https://doi.org/10.4028/www.scientific.net/AMM.215-216.766.
Yang, C., Dong, H., Hu, Z., 2018. Micro-mechanism of central damage formation during cross wedge rolling. J. Mater. Process. Technol. 252, 322–332 https://doi.org/10.1016/j.jmatprotec.2017.09.041.
Zhou, J., Xiao, C., Yu, Y.Y., Jia, Z., 2012. Influence of tool parameters on central deformation in two-wedge two-roll cross-wedge rolling. Adv. Mat. Res. 486, 478–483. https://doi.org/10.4028/www.scientific.net/AMR.486.478.
Zhou, X., Shao, Z., Pruncua, C.I., Hua, L., Balint, D., Lin, J., Jiang, J., 2020a. A study on central crack formation in cross wedge rolling. J. Mat. Process. Technol. 279, 116549 https://doi.org/10.1016/j.jmatprotec.2019.116549.
Zhou, X., Shao, Z., Zhang, C., Sun, F., Zhou, W., Hua, L., Jiang, J., Wang, L., 2020b. The study of central cracking mechanism and criterion in cross wedge rolling. Int. J. Mach. Tools Manuf. 159, 103647 https://doi.org/10.1016/j.ijmachtools.2020.103647.